Efficient Computation of the Linear Radiation Problem using a Spectral Element Method

Jens Visbech[1], **Allan P. Engsig-Karup**[1], **and Harry B. Bingham**[2]
[1] Department of Applied Mathematics and Computer Science
[2] Department of Mechanical Engineering
Technical University of Denmark, 2800 Kgs. Lyngby, Denmark
s161975@student.dtu.dk or jenshaakon@gmail.com

1 INTRODUCTION

Estimating the hydrodynamic characteristics of bodies interacting with ocean waves is of key importance in ocean engineering. Solving the wave-structure interaction problem has been a topic of research for many years, especially using linearized potential flow theory which generally captures the majority of the physics for typical marine structures. Linear theory allows for a decomposition of the potential into radiation and diffraction parts, where the focus of this abstract lies on the former.

For modelling the linear interactions between floating bodies and ocean waves, the impulsive time-domain formulation has been widely used and studied [1], and in recent years the pseudo-impulsive approach has gained renewed attention [2]. The basic concept for these impulsive methods is to force the floating object with an impulse (or pseudo-impulse) in velocity and measure the resultant force on the body. The Fourier transform of the force divided by the Fourier transform of the body motion conveniently determines the added mass and damping coefficients for all frequencies.

Despite the work by Robertson & Sherwin (1999) [3] suggesting an inherent mesh-instability problem with the spectral element method (SEM) applied to free surfaces waves, significant progress for pure wave propagation and wave-structure interaction using SEM have been made over the last half-decade starting with Engsig-Karup, Eskilsson & Bigoni (2016) [4]. Using this high-order numerical discretization method allows for exceptional geometrical flexibility, high accuracy and efficiency, and an optimal $\mathcal{O}(n)$ scaling of the computational effort. This latter property is achieved in combination with p-multigrid techniques [5, 6]. For a further review of the SEM and its beneficial capabilities see [7].

This abstract seeks to highlight recent progress towards developing a computational tool in the setting of linear potential flow using a pseudo-impulsive approach combined with a higher-order SEM. This ultimately enables all of the aforementioned features of this numerical method, including curvilinear elements, unstructured meshes, different radiation conditions, and much more.

2 GOVERNING EQUATIONS

In a general 3D setting, $d = 3$, an Eulerian Cartesian coordinate system is adopted, where the xy-axis represents the horizontal plane, and the vertical z-axis is defined as positive in the upwards direction. These axes span the entire fluid domain, $\Omega \subset \mathbb{R}^d$, which is bounded by the free surface (FS), $\Gamma^{FS} \subset \mathbb{R}^{d-1}$, and the bathymetry, $\Gamma^b \subset \mathbb{R}^{d-1}$. Also, Ω is bounded by the the body surface, $\Gamma^{body} \subset \mathbb{R}^{d-1}$, the far-field boundary, $\Gamma^\infty \subset \mathbb{R}^{d-1}$, and potentially also a symmetry boundary, $\Gamma^{sym} \subset \mathbb{R}^{d-1}$. The depth is denoted by $z = -h(\boldsymbol{x})$, where $\boldsymbol{x} = (x, y)$, and the free surface is defined as $z = \eta(\boldsymbol{x}, t)$, where the time domain is $T : t \geq 0$. Notations for the 2D setting are illustrated in Figure 1.

Applying the theory of linear potential flow, enables the general solution for wave-structure interactions to be decomposed into independently solvable parts, where the focus of this abstract lies upon the k radiation potentials, ϕ_k. In the following, we will use the notation: $\nabla = (\partial_x, \partial_y)$, where e.g. ∂_x is the derivative with respect to x.

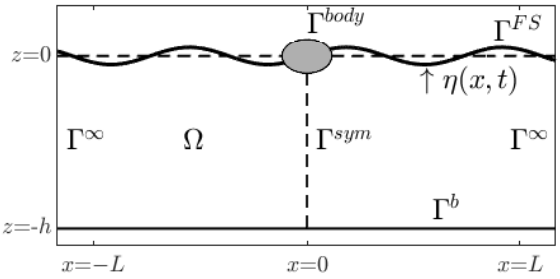

Figure 1: Notations for the 2D physical domain, Ω.

The temporal development is governed by the linearized kinematic and dynamic free surface boundary conditions

$$\partial_t \eta = \tilde{w}_k \quad \text{and} \quad \partial_t \tilde{\phi}_k = -g\eta \quad \text{on} \quad \Gamma^{FS}, \tag{1}$$

where the "$\sim$"-notation indicates quantities evaluated on Γ^{FS}, i.e. $\tilde{\phi}_k = \phi_k(\boldsymbol{x}, 0, t)$ and $\tilde{w}_k = \partial_z \phi_k|_{z=0}$.

Combined with the free surface conditions, the continuity equation, in the form of a Laplace problem, governs the spatial domain with an in-homogeneous Dirichlet boundary condition on Γ^{FS} and a homogeneous Neumann boundary condition on Γ^b,

$$(\nabla, \partial_z)^2 \phi_k = 0 \quad \text{for} \quad -h \leq z \leq 0, \tag{2}$$

$$\phi_k = \tilde{\phi}_k \quad \text{on} \quad \Gamma^{FS}, \quad \text{and} \quad \partial_n \phi_k = 0 \quad \text{on} \quad \Gamma^b, \tag{3}$$

where ∂_n is the derivative in the normal direction to the boundary. For the body boundary condition on Γ^{body}:

$$\partial_n \phi_k = \dot{\xi}_k n_k \quad \text{on} \quad \Gamma^{body}, \quad \text{where } n_k = \begin{cases} \boldsymbol{n} & k = 1,2,3 \\ \boldsymbol{r} \times \boldsymbol{n} & k = 4,5,6 \end{cases} \tag{4}$$

in which $\boldsymbol{n}$ is the normal vector and $\boldsymbol{r}$ is the position vector of a point on Γ^{body}. Furthermore, ξ_k denotes the displacement of the body, which is to be modelled as a Gaussian, so that a tailored frequency content governed by the spatial resolution, is released into the system. See [2] for more details. The Gaussian should be modelled in such a way that the displacement at $t = 0$, is practically zero, which in combination with a zero-imposed velocity potential at the free surface, will form the initial conditions for (1).

It can be computationally beneficial to impose a symmetry boundary, Γ^{sym}, on the symmetry-axis of the body. For symmetrical and anti-symmetrical problems these are given as

$$\partial_{\boldsymbol{x}} \phi_k = 0 \quad \text{or} \quad \phi_k = 0 \quad \text{on} \quad \Gamma^{sym}. \tag{5}$$

On the far-field boundary, Γ^{∞}, appropriate actions should be taken to avoid reflections that could influence the frequency content of the solution. Combinations of various approaches have been used: 1) a simple grid stretching technique, 2) classical relaxation zone techniques, and/or 3) an in-homogeneous Neumann-type Sommerfeld boundary condition.

2.1 Added mass and damping coefficients

From [2] it can be shown that the added mass and damping coefficients can be computed via the Fourier transform, $\mathcal{F}(\cdot)$, of the discrete displacement and force time signals as

$$\omega^2 a_{jk} - \mathrm{i}\omega b_{jk} = \frac{\mathcal{F}\{F_{jk}(t)\}}{\mathcal{F}\{\xi_k(t)\}}, \tag{6}$$

where $F_{jk}(t)$ is the radiation force for mode j caused by an impulse in mode k. This can be computed by integrating the linear dynamic pressure over the wetted body surface, Γ^{body}.

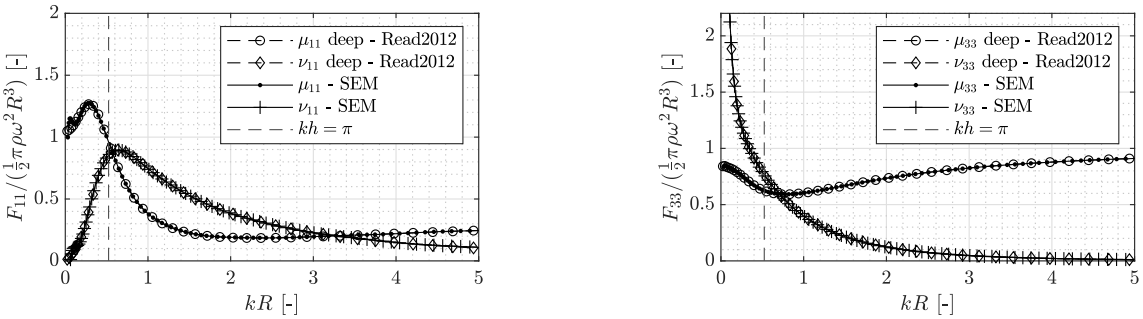

Figure 2: Numerical results for a surging (left) and a heaving (right) cylinder using 4th order polynomials.

3 NUMERICAL SOLUTION

The Laplace problem given by (2) and its associated boundary conditions are discretized using the SEM in a 2D setting, hereby splitting the fluid domain, Ω, into non-overlapping triangular elements with curvilinear sides - if needed - in an unstructured way so that the mesh is more refined at Γ^{FS} and Γ^{body} than in the rest of the spatial domain. On this discrete domain, global piece-wise continuous polynomial finite element basis functions of order P will represent the solution, thus leading to a sparse linear system of equations

$$\boldsymbol{A}\boldsymbol{\phi_k} = \boldsymbol{b}, \quad \boldsymbol{A} \in \mathbb{R}^{DOF \times DOF}, \quad \boldsymbol{b} \in \mathbb{R}^{DOF}. \tag{7}$$

The governing temporal equations given by (1) will be evolved in time using a classical explicit four-stage Runge-Kutta time integration scheme in combination with a conservative global CFL condition to ensure conditional stability. The time steep is chosen to be $\Delta t = \frac{\mathrm{Cr}\,\Delta x_{\min}}{u_{\max}}$, where Cr is the Courant number, $\mathrm{Cr} \in [0.5\ ;\ 1]$, $\Delta x_{\min}$ is the minimum grid spacing on the free surface elements, and $u_{\max}$ is the asymptotic limit of the linear wave celerity, i.e. $u_{\max} = \sqrt{g/k\tanh(kh)}$.

The evaluation of the time derivatives in the Bernoulli equation for the pressure are computed by finite difference schemes with fourth-order accuracy to accordance with the time integration scheme. Finally, the Fourier transforms in (6) are evaluated using a fast Fourier transform.

4 NUMERICAL CASES AND RESULTS

At present moment, the 2D implementation has been validated extensively by achieving spectral convergence (fixed mesh and increasing polynomial order) and algebraic convergence rates (fixed polynomial order and decreasing uniform element sizes) for affine and curvilinear triangular elements, on structured and unstructured meshes. Also, the solver has been validated against different known benchmarks. A 3D implementation is in progress from which results will be presented at the workshop including the aforementioned validation analysis.

The case studies that are presented are heavily inspired by those presented in [8] using a finite difference solver, hence showing normalised results for a half-submerged cylinder (radius: $R = 0.5$ and depth: $h = 3$). The finite difference solver [8] on an overset grid was validated against analytical infinite-depth solutions calculated using a multipole method.

From Figure 2 the surge-surge and heave-heave results in terms of non-dimensional added mass and damping coefficients for a cylinder are plotted with the numerical results from [8]. The results show excellent visual agreement, ultimately confirming the legitimacy and correctness of the SEM model. Similar results were obtained for the barge case from the reference abstract.

To show the promising geometrical flexibility features of the model, a simple 2D version of a tetra spar buoy has been implemented, see Figure 3. A symmetry boundary, Γ^{sym}, is applied on the left boundary. The geometry of the structure is: Top part is $B = 10$ m wide, straight vertical part is B long, length of leg (measured at the top part of each leg) is $3B$, width of the leg is $B/4$, and angle between the legs is $\pi/2$.

The added mass and damping coefficients are given in non-dimensional form by

$$\tilde{a}_{jk} = \frac{a_{jk}}{\frac{1}{2}\pi\rho L_c^2}, \quad \tilde{b}_{jk} = \frac{b_{jk}}{\frac{1}{2}\pi\rho\omega L_c^2}, \tag{8}$$

where L_c is a characteristic length of the structure taken to be the leg length, $L_c = 3B$.

The preliminary results for this geometrically demanding structure are shown in Figure 4.

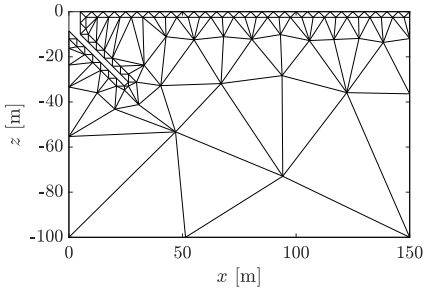

Figure 3: Illustration of an unstructured mesh for a 2D simplified version of a 3D tetra spar bouy.

5 ACKNOWLEDGEMENTS

The computations were performed on resources provided by the DTU Computing Center (DCC) at the Technical University of Denmark.

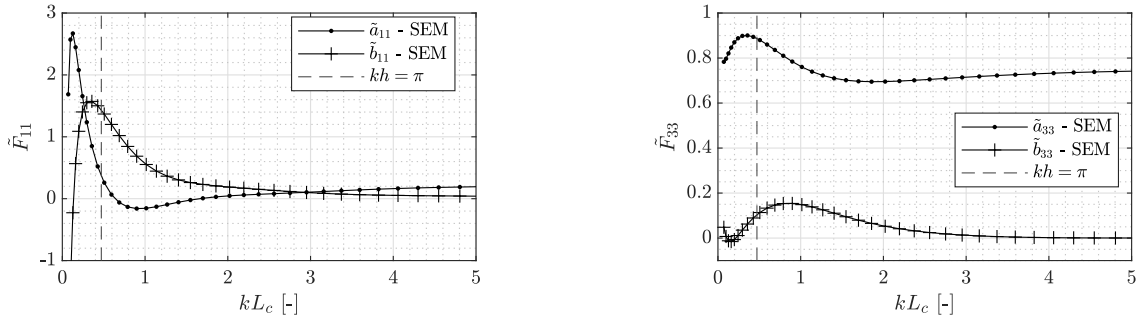

Figure 4: Numerical results for surging (left) and a heaving (right) 2D tetra spar buoy geometry with $h = 20B$.

REFERENCES

[1] Bingham, H. B. 1994. *Simulating ship motions in the time domain.* PhD thesis, Massachusetts Institute of Technology.

[2] Amini-Afshar, M., and Bingham, H. B. 2017. *Solving the linearized forward-speed radiation problem using a high-order finite difference method on overlapping grids.* Applied Ocean Research 69(1), 220–244.

[3] Robertson, I., and Sherwin, S. 1999. *Free-surface flow simulation using hp/spectral elements.* Journal of Computational Physics 155(1), 26–53.

[4] Engsig-Karup, A., Eskilsson, C., and Bigoni, D. 2016. *A stabilised nodal spectral element method for fully nonlinear water waves.* Journal of Computational Physics 318(1), 1–21.

[5] Engsig-Karup, A. P., and Laskowski, W. L. 2021. *An efficient p-multigrid spectral element model for fully nonlinear water waves and fixed bodies.* Int. J. Num. Meth. Fluids 93(9), 2823–2841.

[6] Mortensen, L., Laskowski, W., Engsig-Karup, A., Eskilsson, C., and Monteserin, C. Simulation of nonlinearwaves interacting with a heaving body using a *p*-multigrid spectral element method. In *The 31st International Ocean and Polar Engineering Conference* (2021), OnePetro.

[7] Xu, H., Cantwell, C., Monteserin, C., Eskilsson, C., Engsig-Karup, A., and Sherwin, S. 2018. *Spectral/hp element methods: Recent developments, applications, and perspectives.* Journal of Hydrodynamics 30(1), 1–22.

[8] Read, R., and Bingham, H. B. 2012. *Solving the linear radiation problem using a volume method on an overset grid. IWWWFB27.*